

MULTI-MICROPHONE COMPLEX SPECTRAL MAPPING FOR SPEECH DEREVERBERATION

Zhong-Qiu Wang¹ and DeLiang Wang^{1,2}

¹Department of Computer Science and Engineering, The Ohio State University, USA

²Center for Cognitive and Brain Sciences, The Ohio State University, USA

{wangzhon, dwang}@cse.ohio-state.edu

ABSTRACT

This study proposes a multi-microphone complex spectral mapping approach for speech dereverberation on a fixed array geometry. In the proposed approach, a deep neural network (DNN) is trained to predict the real and imaginary (RI) components of direct sound from the stacked reverberant (and noisy) RI components of multiple microphones. We also investigate the integration of multi-microphone complex spectral mapping with beamforming and post-filtering. Experimental results on multi-channel speech dereverberation demonstrate the effectiveness of the proposed approach.

Index Terms—Beamforming, complex spectral mapping, speech dereverberation, microphone array processing, deep learning.

1. INTRODUCTION

Microphone array processing is pervasive in modern hands-free speech communication systems such as smart speakers and phones. With multiple microphones, spatial information can be leveraged in addition to spectral cues to improve speech enhancement and audio source separation. Conventionally, multi-microphone beamforming followed by monaural post-filtering is the most popular approach for multi-channel speech enhancement [1]–[4]. This approach requires an accurate estimate of target direction, and power spectral density and covariance matrices of speech and noise. The estimation is traditionally performed by using for example non-negative matrix factorization or maximum likelihood estimation under a hypothesized probabilistic distribution. Recently, riding on the development of DNN, time-frequency (T-F) masking and mapping based approaches have been established as the main approaches for single-channel speech enhancement and speaker separation [2], [5]–[7]. These studies suggest that deep learning can substantially improve magnitude estimation. In addition, such mask or magnitude estimation provides a powerful means for acoustic beamforming [8], [9] and sound source localization [10]. As a mask value at a T-F unit is close to one, the phase at that unit is little contaminated. Such T-F units can therefore be utilized to robustly compute the covariance matrix of each source for beamforming and localization.

In the line of research on masking-based beamforming, earlier efforts [8], [10]–[14] only use DNN on spectral features to compute a mask for each microphone, and the estimated masks at different microphones are then pooled together to identify T-F units dominated by the same source across all the microphones for covariance matrix computation. Subsequent studies incorporate spatial features such as inter-channel phase differences (IPD) [15], [16], cosine and sine IPD, target direction compensated IPD [17], beamforming results [18], [19], and stacked phases and magnitudes [20], [21] as a way of leveraging spatial information to further improve mask estimation for beamforming. However, these studies aim at improving mask or magnitude estimation, and do not address phase estimation.

In addition, many studies assume a relatively blind setup, where the trained models are designed to be directly applicable to arrays with any number of microphones arranged in an unknown geometry. Although this flexibility is desirable, in applications such as

Amazon Echo and Google Home, the device only has a fixed microphone array with a known number of microphones and geometry. How to leverage this fixed geometry for robust speech processing is therefore an interesting research problem to investigate.

As an initial step towards multi-channel speech enhancement, this study proposes a multi-microphone complex spectral mapping approach for speech dereverberation based on a fixed array geometry, where the real and imaginary (RI) components of multiple microphones are concatenated as input features for a DNN to predict the RI components of the direct-path signal(s) captured at a reference microphone or at all the microphones. The initially estimated target speech can be utilized to compute a beamformer, and the RI components of the beamforming results can be further combined with the RI components of all the microphone signals for post-filtering.

Why should this approach work? We believe that, for a fixed-geometry array, the neural network could learn to enhance the speech arriving from a specific direction by exploiting the spatial information contained in multiple microphones. This approach is in a way similar to recent studies of classification-based sound source localization for arrays with fixed geometry, where a DNN is trained to learn a one-to-one mapping from the inter-channel phase patterns of multiple microphones to the target direction [22]–[25]. Based on deep learning, the proposed approach has the potential to model the non-linear spatial information contained in multi-microphone inputs, while conventional beamforming is only linear and typically utilizes second-order statistics [1] within each frequency.

Although there are time-domain approaches that use multi-microphone modeling for speech enhancement and source separation [26]–[28], their effectiveness in environments with moderate to strong reverberation is not yet established [29]. In addition, our study tightly integrates multi-microphone complex spectral mapping with beamforming and post-filtering.

The rest of this paper presents the physical model and proposed algorithms in Sections 2 and 3, experimental setup and evaluation results in Sections 4 and 5, and conclusions in Section 6.

2. PHYSICAL MODELS AND OBJECTIVES

Given a P -channel signal recorded in a noisy reverberant environment, the physical model in the short-time Fourier transform (STFT) domain can be formulated as

$$\begin{aligned} \mathbf{Y}(t, f) &= \mathbf{c}(f; p)S_q(t, f) + \mathbf{H}(t, f) + \mathbf{N}(t, f) \\ &= \mathbf{S}(t, f) + \mathbf{V}(t, f) \end{aligned} \quad (1)$$

where $S_q \in \mathbb{C}$ is the target speech capture by a reference microphone q , $\mathbf{c}(f; q) \in \mathbb{C}^{P \times 1}$ is the relative transfer function with the q^{th} element being one, $\mathbf{Y}(t, f)$, $\mathbf{c}(f; p)S_q(t, f)$, $\mathbf{H}(t, f)$, and $\mathbf{N}(t, f) \in \mathbb{C}^{P \times 1}$ respectively represent the STFT vectors of the mixture, direct sound, reverberation, and reverberant noise. We aim at recovering S_q based on \mathbf{Y} . Our study focuses on dereverberation and the noise is assumed to be an air-conditioning noise, although the proposed approach can be readily applied to deal with more challenging noises. We use \mathbf{S} to denote the target speech to extract and \mathbf{V} the non-target speech to remove. Our study assumes an offline processing scenario. We normalize the sample variance of each

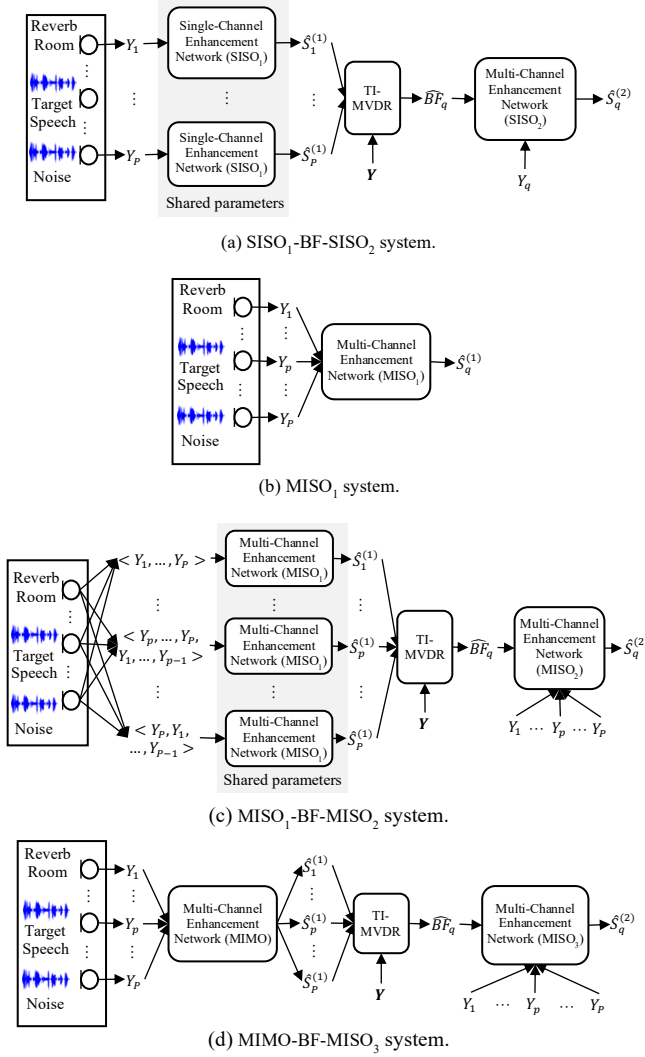


Figure 1. System overview.

microphone signal to one before any processing. This can deal with random gains in input. We also assume that the same microphone array is used for training and testing.

3. PROPOSED ALGORITHMS

We propose four approaches (denoted as SISO₁-BF-SISO₂, MISO₁, MISO₁-BF-MISO₂, and MIMO-BF-MISO₃, see Figure 1) for multi-channel speech dereverberation. This section discusses each one of them and their combination with beamforming and post-filtering.

3.1. SISO₁-BF-SISO₂ System

The SISO₁-BF-SISO₂ system contains two single-input and single-output (SISO) networks. The first one (SISO₁) performs single-channel complex spectral mapping at each microphone. The enhanced speech is used to compute a time-invariant minimum variance distortion-less response (TI-MVDR) beamformer. The beamforming result \widehat{BF}_q is then combined with the mixture at the reference microphone Y_q as the input to the second SISO network (SISO₂) for complex spectral mapping based post-filtering. Note that the trained models of this approach can be applied to arrays with any number of microphones arranged in an unknown geometry.

Following [30]–[32], we train a DNN to directly predict the RI components of the direct-path signal from noisy and reverberant ones via complex spectral mapping. The loss function is

$$\mathcal{L}_{p,RI} = \|\widehat{R}_p - \text{Real}(S_p)\|_1 + \|\widehat{I}_p - \text{Imag}(S_p)\|_1 \quad (2)$$

where p indexes microphones, \widehat{R}_p and \widehat{I}_p are the predicted RI components, and $\text{Real}(\cdot)$ and $\text{Imag}(\cdot)$ extract RI components. The enhanced speech is computed as $\widehat{S}_p^{(k)} = \widehat{R}_p^{(k)} + j\widehat{I}_p^{(k)}$. The superscript $k \in \{1,2\}$ denotes it is produced by the k^{th} DNN (see Figure 1(a)).

Following recent studies [31], [33] that include a magnitude-domain loss for complex spectra approximation, we design the following loss function

$$\mathcal{L}_{p,RI+Mag} = \mathcal{L}_{p,RI} + \||\widehat{S}_p| - |S_p|\|_1 \quad (3)$$

The motivation is that using $\mathcal{L}_{p,RI}$ alone produces worse magnitude estimates, as the estimated magnitudes need to compensate for the estimation error of phase. A major difference from [31], [33] is that we do not perform power or logarithmic compression on the magnitude spectra. This way, the DNN is always trained to estimate an STFT spectrogram that has consistent phase and magnitude structure, and hence would likely produce a good consistent STFT spectrogram at run time [34], [35].

3.2. MISO₁ System

The multiple-input and single-output system (denoted as MISO₁) stacks the RI components of the mixtures at all the microphones and predicts the RI components of the direct-path signal at a reference microphone. This algorithm essentially trains a DNN for non-linear time-varying beamforming. It is simple, fast, and can be easily modified for real-time processing. The model is trained using $\mathcal{L}_{q,RI+Mag}$.

We emphasize that conventional multi-channel Wiener filtering computes a linear filter per frequency or per T-F unit to project the mixture $\mathbf{Y}(t, f)$ onto $S_q(t, f)$, typically based on second-order statistics [1]. In contrast, we utilize a DNN to learn a highly non-linear function to map \mathbf{Y} to S_q . Although this seems challenging for arrays with arbitrary geometry, for a fixed geometry, this could work as the inter-channel phase patterns are almost fixed for the signal arriving from a specific direction.

3.3. MISO₁-BF-MISO₂ System

The MISO₁-BF-MISO₂ system includes a MISO network, an MVDR beamformer, and another MISO network. This system is similar to SISO₁-BF-SISO₂, but we use two MISO networks rather than two SISO networks, since MISO is expected to be better than SISO by doing multi-microphone modeling.

We circularly shift the microphones to estimate the direct-path signal at each microphone. For example, we stack an ordered microphone sequence $\langle Y_1, \dots, Y_p \rangle$ as the inputs to MISO₁ to obtain $\widehat{S}_1^{(1)}$, and feed in $\langle Y_p, \dots, Y_p, Y_1, \dots, Y_{p-1} \rangle$ to obtain $\widehat{S}_p^{(1)}$. This strategy would work as we use a circular array with uniformly spaced microphones.

An MVDR beamformer is then computed using $\widehat{\mathbf{S}}$. The beamforming result \widehat{BF}_q is combined with \mathbf{Y} to predict S_q using a MISO network (denoted as MISO₂) via complex spectral mapping. This way, post-filtering can also leverage multi-microphone modeling.

3.4. MIMO-BF-MISO₃ System

The MIMO-BF-MISO₃ system consists of a multiple-input and multiple-output (MIMO) network, an MVDR beamformer, and a MISO

network. The MIMO network takes in the mixture RI components of all the microphones to predict the RI components of the direct-path signals at all the microphones. This way, we can get an estimate of \mathbf{S} for beamforming by performing feed-forwarding only once, rather than P times as in SISO₁-BF-SISO₂ and MISO₁-BF-MISO₂. The amount of computation is therefore dramatically reduced. The loss function for the MIMO network is

$$\mathcal{L}_{1,\dots,P,\text{RI+Mag+PhaseDiff}} = \frac{1}{P} \sum_{p=1}^P \mathcal{L}_{p,\text{RI+Mag}} + \frac{1}{P^2 - P} \sum_{p'=1}^P |S_{p'}| \sum_{p''=1}^P \left(1 - \cos(\angle \hat{S}_{p'} - \angle \hat{S}_{p''} - (\angle S_{p'} - \angle S_{p''})) \right) / 2 \quad (4)$$

where the second term is a magnitude-weighted cosine distance between the predicted phase differences and the actual phase differences of all the microphone pairs. In our experiments, the second term leads to faster convergence and better performance over using the first term alone.

After obtaining $\hat{\mathbf{S}}$, we compute an MVDR beamformer. The beamforming result $\hat{B}\hat{F}_q$ is combined with \mathbf{Y} to predict S_q using a MISO network (denoted as MISO₃) via complex spectral mapping.

3.5. MVDR Beamforming

SISO₁-BF-SISO₂, MISO₁-BF-MISO₂ and MIMO-BF-MISO₃ all have a beamforming module. We use the estimated complex spectra produced by complex spectral mapping to directly compute the speech and noise covariance matrices for TI-MVDR beamforming.

$$\hat{\Phi}^{(s)}(f) = \frac{1}{T} \sum_{t=1}^T \hat{\mathbf{S}}(t, f) \hat{\mathbf{S}}(t, f)^H \quad (5)$$

$$\hat{\Phi}^{(v)}(f) = \frac{1}{T} \sum_{t=1}^T \hat{\mathbf{V}}(t, f) \hat{\mathbf{V}}(t, f)^H$$

where $\hat{\mathbf{V}} = \mathbf{Y} - \hat{\mathbf{S}}$. Previous neural beamforming approaches usually select T-F units dominated by direct sound for covariance matrix estimation by using a T-F mask to compute a weighted sum of all the mixture outer products $\mathbf{Y}(t, f)\mathbf{Y}(t, f)^H$ within each frequency [8], [10]–[12]. In contrast, we use the estimated complex spectra directly. The rationale is that there may be insufficient T-F units dominated by direct sound especially when room reverberation is very strong, and the phase produced by complex spectral mapping is expected to be better than the mixture phase.

We consider TI-MVDR, as the sound source is assumed to be non-moving within each utterance, and reverberation and the considered noise is largely diffuse. The relative transfer function is computed as follows

$$\hat{\mathbf{r}}(f) = \mathcal{P}\{\hat{\Phi}^{(s)}(f)\} \quad (6)$$

$$\hat{\mathbf{c}}(f; q) = \hat{\mathbf{r}}(f) / \hat{r}_q(f) \quad (7)$$

where $\mathcal{P}\{\cdot\}$ extracts the principal eigenvector [1]. We use Eq. (7) to compute the relative transfer function with respect to a reference microphone q .

An MVDR beamformer is computed as

$$\hat{\mathbf{w}}(f; q) = \frac{\hat{\Phi}^{(v)}(f)^{-1} \hat{\mathbf{c}}(f; q)}{\hat{\mathbf{c}}(f; q)^H \hat{\Phi}^{(v)}(f)^{-1} \hat{\mathbf{c}}(f; q)} \quad (8)$$

Beamforming results are obtained as $\hat{B}\hat{F}_q(t, f) = \hat{\mathbf{w}}(f; q)^H \mathbf{Y}(t, f)$.

4. EXPERIMENTAL SETUP

We use the WSJ0CAM corpus and a large set of simulated room impulse responses (RIRs, in total 39,305 eight-channel RIRs) to simulate room reverberation. See Algorithm 1 for the detailed procedure. For each utterance, we randomly generate a room with different room characteristics, microphone and speaker locations, array configurations, and noise levels. Our study considers an eight-

Input: WSJCAM0;

Output: spatialized reverberant (and noisy) WSJCAM0;

For *dataset*, *REP* in {*train:5, validation:4, test:3*} set of WSJCAM0 **do**

For each anechoic speech signal *s* in *dataset* **do**

Repeat *REP* times **do**

- Draw room length r_x and width r_y from [5,10] m, and height r_z from [3,4] m;

- Sample mic array height a_z from [1,2] m;

- Sample array displacement n_x and n_y from [-0.5,0.5] m;

- Place array center at $(\frac{r_x}{2} + n_x, \frac{r_y}{2} + n_y, a_z)$ m;

- Set array radius a_r to 0.1 m;

- Sample angle of first mic θ from $[0, \frac{\pi}{4}]$;

- Place P ($= 8$) mics uniformly on the circle, starting from angle θ ;

- Sample target speaker locations: $(s_x, s_y, s_z (= a_z))$ such that distance

from target speaker to array center is in between [0.75,2.5] m, and target speaker is at least 0.5 m from each wall;

- Sample T60 from [0.2,1.3] s;

- Generate multi-channel impulse responses and convolve them with *s*;

If *dataset* in {*train, validation*} **do**

- Sample a P -channel noise signal *n* from REVERB training noise;

Else

- Sample a P -channel noise signal *n* from REVERB testing noise;

End

- Concatenate channels of reverberated *s* and *n* respectively, scale them to an SNR randomly sampled from [5,25] dB, and mix them;

End

End

Algorithm 1. Data spatialization process.

microphone circular array with the radius fixed at 10 cm. The target speaker is in the same plane as the array, at a distance sampled from [0.75,2.5] m. The training and testing noise (mostly air-conditioning noise) used in the REVERB challenge [36] is utilized to simulate noisy-reverberant mixtures for training and testing, respectively. The reverberation time (T60) is randomly drawn from the range [0.2,1.3] s. The average direct-to-reverberation energy ratio is -3.7 dB with 4.4 dB standard deviation. There are 39,305 (7,861×5, ~80 h), 2,968 (742×4, ~6 h) and 3,264 (1,088×3, ~7 h) eight-channel utterances in the training, validation and test set, respectively.

We validate our algorithms on speech dereverberation using one, two and four microphones. We use the first microphone for the single-microphone task, the first and fifth for the two-microphone task, and the first, third, fifth and seventh for the four-microphone task. Note that the two- and four-microphone setups both have an aperture size of 20 cm. The first microphone is considered as the reference microphone for metric computation. We use scale-invariant SDR (SI-SDR) [37] and PESQ as the evaluation metrics. The former closely reflects the accuracy of estimated magnitude and phase, meaning that estimated magnitude and phase need to compensate with each other to produce a higher SI-SDR, and the latter strongly correlates with the quality of estimated magnitudes.

To evaluate the generalization ability of the trained models, we directly apply them to the recorded data of REVERB [36] for automatic speech recognition (ASR). The recording device is an eight-microphone circular array with 10 cm radius. Note that the array geometry is subject to manufacturing error, which introduces a geometry mismatch between training and testing. The T60 is around 0.7 s and the speaker-to-array distance is 1 m in the near-field case and 2.5 m in the far-field case. We always consider the first microphone as the reference microphone. The ASR backend is built using the most recent Kaldi toolkit.

We use a two-layer BLSTM with convolutional U-Net structure [38], skip connections and dense blocks [39] for dereverberation. See Figure 2 for an illustration of for example the MISO₂ network. The rationale for this network design [40] is that BLSTM can model long-range dependencies along time, U-Net can maintain fine-grained structure and exploit large receptive fields, and dense blocks encourage feature re-use and improve the discriminative power of

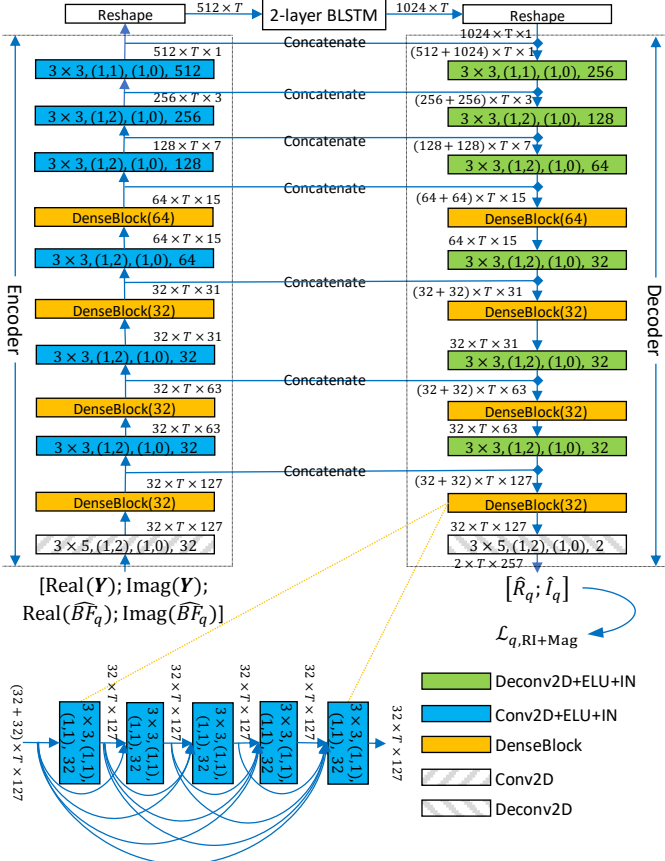


Figure 2. Network architecture of MISO₂ for predicting the RI components of S_q from the RI components of Y and \widehat{BF}_q . The tensor shape after each block is in the format: $featureMaps \times timeSteps \times frequencyChannels$. Each Conv2D, Deconv2D, Conv2D+IN+ELU, and Deconv2D+IN+ELU block is specified in the format: $kernelSizeTime \times kernelSizeFreq, (stridesTime, stridesFreq), (paddingTime, paddingFreq), featureMaps$. Each DenseBlock(g) contains five Conv2D+IN+ELU blocks with growth rate g .

the network. The encoder has one two-dimensional (2D) convolution, and six convolutional blocks, each with 2D convolution, exponential linear units (ELU) and instance normalization (IN), for down-sampling. The decoder contains six convolutional blocks, each with 2D deconvolution, ELU and IN, and one 2D deconvolution, for up-sampling. The RI components of multiple microphones are stacked as feature maps for the network input and output. The window size is 32 ms and hop size 8 ms. The sampling rate is 16 kHz. A 512-point DFT is performed to extract 257-dimensional STFT features at each microphone.

5. EVALUATION RESULTS

Table 1 compares the performance of complex spectral mapping with real-valued masking using estimated spectral magnitude mask (SMM) [2] and phase-sensitive mask (PSM) [41] on monaural dereverberation. Much better SI-SDR is obtained using complex spectral mapping based models trained with \mathcal{L}_{RI} and \mathcal{L}_{RI+Mag} over using estimated SMM and PSM, suggesting that complex spectral mapping is effective at phase estimation. In addition, \mathcal{L}_{RI+Mag} leads to much better PESQ than \mathcal{L}_{RI} , and slightly better SI-SDR. This indicates the importance of magnitude estimation when PESQ is used as the evaluation metric. The magnitude loss is always included for complex spectral mapping in the following experiments.

Table 1. Average SI-SDR (dB) and PESQ of different methods on monaural dereverberation. $T_a^b(\cdot) = \min(\max(\cdot, a), b)$.

Methods	SI-SDR	PESQ
Unprocessed	-3.8	1.93
Estimated SMM	0.6	2.92
Estimated PSM	2.2	2.54
\mathcal{L}_{RI}	6.1	2.79
\mathcal{L}_{RI+Mag}	6.5	3.10
Oracle SMM ($T_0^{10}(S_q / Y_q)$)	1.5	3.39
Oracle PSM ($T_0^1(S_q \cos(\angle S_q - \angle Y_q)/ Y_q)$)	4.4	3.09

Table 2. Average SI-SDR (dB) and PESQ of different methods on two- and four-channel dereverberation using simulated test data, and average word error rates (WER) (%) on REVERB real test data.

Metrics	SI-SDR			PESQ			WER on REVERB		
	1	2	4	1	2	4	1	2	4
#mics									
SISO ₁	6.5	-	-	3.10	-	-	9.62	-	-
SISO ₁ -BF-SISO ₁	-	8.0	9.4	-	3.20	3.29	-	8.37	7.63
SISO ₁ -BF-SISO ₂	-	8.2	10.6	-	3.22	3.38	-	7.96	7.25
MISO ₁	-	7.6	9.0	-	3.22	3.33	-	7.38	6.88
MISO ₁ -BF-MISO ₂	-	8.6	10.9	-	3.24	3.43	-	7.38	6.30
MIMO	-	7.2	7.8	-	3.23	3.33	-	7.46	6.74
MIMO-BF-MISO ₃	-	8.7	10.6	-	3.28	3.41	-	7.92	6.62
WPE	-	-	-	-	-	-	14.01	13.14	11.45
WPE+BeamformIt	-	-	-	-	-	-	-	12.64	9.30

Table 2 first reports the enhancement performance of various multi-channel approaches. SISO₁ represents a baseline of monaural complex spectral mapping. In SISO₁-BF-SISO₁, we apply monaural complex spectral mapping on \widehat{BF}_q to estimate target speech S_q , while in SISO₁-BF-SISO₂, complex spectral mapping is applied on the combination of \widehat{BF}_q and Y_q to estimate S_q as in Figure 1(a). SISO₁-BF-SISO₂ produces better performance than SISO₁-BF-SISO₁ and SISO₁. We emphasize that SISO₁-BF-SISO₁ represents a typical beamforming followed by post-filtering approach in DNN based multi-channel speech enhancement [4]. In addition, both MISO₁ and MIMO are better than SISO₁. This indicates that concatenating multiple microphones for complex spectral mapping clearly helps. MIMO is worse than MISO₁, because producing multiple outputs is a harder task. Overall, MISO₁-BF-MISO₂ and MIMO-BF-MISO₃ perform the best. This is likely because MISO networks used for post-filtering can benefit from multi-microphone modeling.

In Table 2 we also evaluate the trained models in terms of ASR performance directly on the real test set of REVERB. Both MISO₁-BF-MISO₂ and MIMO-BF-MISO₃ exhibit strong generalization ability, and better ASR performance than SISO₁-BF-SISO₁ and SISO₁-BF-SISO₂, which are not sensitive to geometry mismatch. Clear improvements are observed using the trained models over the baseline weighted prediction error (WPE) [36] and WPE followed by BeamformIt algorithms, both available in Kaldi.

6. CONCLUSION

We have proposed a multi-microphone complex spectral mapping approach for speech dereverberation, and integrated it with beamforming and post-filtering into a unified system. Experimental results suggest that on a fixed geometry, concatenating multiple microphone signals for complex spectral mapping leads to clear improvements over using a single channel. Future research will consider its extensions to speech enhancement and speaker separation in reverberant and noisy conditions, and investigate its sensitivity to geometry mismatch. We shall also extend the proposed systems to arrays with more than four microphones.

7. REFERENCES

- [1] S. Gannot, E. Vincent, S. Markovich-Golan, and A. Ozerov, "A Consolidated Perspective on Multi-Microphone Speech Enhancement and Source Separation," *IEEE/ACM Trans. Audio, Speech, Lang. Process.*, vol. 25, pp. 692–730, 2017.
- [2] D. L. Wang and J. Chen, "Supervised Speech Separation Based on Deep Learning: An Overview," *IEEE/ACM Trans. Audio, Speech, Lang. Process.*, vol. 26, pp. 1702–1726, 2018.
- [3] B. Cauchi *et al.*, "Combination of MVDR Beamforming and Single-Channel Spectral Processing for Enhancing Noisy and Reverberant Speech," *EURASIP J. Adv. Signal Process.*, 2015.
- [4] Z.-Q. Wang and D. L. Wang, "All-Neural Multi-Channel Speech Enhancement," in *Proceedings of Interspeech*, 2018, pp. 3234–3238.
- [5] Y. Wang and D.L. Wang, "Towards Scaling Up Classification-Based Speech Separation," *IEEE Trans. Audio. Speech. Lang. Processing*, vol. 21, no. 7, pp. 1381–1390, 2013.
- [6] J. R. Hershey, Z. Chen, J. Le Roux, and S. Watanabe, "Deep Clustering: Discriminative Embeddings for Segmentation and Separation," in *IEEE International Conference on Acoustics, Speech and Signal Processing*, 2016, pp. 31–35.
- [7] M. Kolbæk, D. Yu, Z.-H. Tan, and J. Jensen, "Multi-Talker Speech Separation with Utterance-Level Permutation Invariant Training of Deep Recurrent Neural Networks," *IEEE/ACM Trans. Audio, Speech, Lang. Process.*, vol. 25, no. 10, pp. 1901–1913, 2017.
- [8] J. Heymann, L. Drude, A. Chinaev, and R. Haeb-Umbach, "BLSTM Supported GEV Beamformer Front-End for the 3rd CHiME Challenge," in *IEEE Workshop on Automatic Speech Recognition and Understanding*, 2015, pp. 444–451.
- [9] J. Barker, R. Marxer, E. Vincent, and S. Watanabe, "The Third 'CHiME' Speech Separation and Recognition Challenge: Analysis and Outcomes," *Comput. Speech Lang.*, vol. 46, pp. 605–626, 2017.
- [10] Z.-Q. Wang, X. Zhang, and D. L. Wang, "Robust Speaker Localization Guided by Deep Learning Based Time-Frequency Masking," *IEEE/ACM Trans. Audio, Speech, Lang. Process.*, vol. 27, no. 1, pp. 178–188, 2019.
- [11] H. Erdogan *et al.*, "Improved MVDR Beamforming using Single-Channel Mask Prediction Networks," in *Proceedings of Interspeech*, 2016, pp. 1981–1985.
- [12] X. Zhang, Z.-Q. Wang, and D. L. Wang, "A Speech Enhancement Algorithm by Iterating Single- and Multi-Microphone Processing and Its Application to Robust ASR," in *IEEE International Conference on Acoustics, Speech and Signal Processing*, 2017, pp. 276–280.
- [13] T. Ochiai, S. Watanabe, T. Hori, and J. R. Hershey, "Multichannel End-to-End Speech Recognition," in *Proceedings of ICML*, 2017.
- [14] H. Taherian, Z.-Q. Wang, and D. L. Wang, "Deep Learning Based Multi-Channel Speaker Recognition in Noisy and Reverberant Environments," in *Proceedings of Interspeech*, 2019, pp. 4070–4074.
- [15] Z.-Q. Wang, J. Le Roux, and J. R. Hershey, "Multi-Channel Deep Clustering: Discriminative Spectral and Spatial Embeddings for Speaker-Independent Speech Separation," in *IEEE International Conference on Acoustics, Speech and Signal Processing*, 2018, pp. 1–5.
- [16] T. Yoshioka, H. Erdogan, Z. Chen, and F. Alleva, "Multi-Microphone Neural Speech Separation for Far-Field Multi-Talker Speech Recognition," in *IEEE International Conference on Acoustics, Speech and Signal Processing*, 2018, pp. 5739–5743.
- [17] Z.-Q. Wang and D. L. Wang, "On Spatial Features for Supervised Speech Separation and Its Application to Beamforming and Robust ASR," in *IEEE International Conference on Acoustics, Speech and Signal Processing*, 2018, pp. 5709–5713.
- [18] Z.-Q. Wang and D. L. Wang, "Integrating Spectral and Spatial Features for Multi-Channel Speaker Separation," in *Proceedings of Interspeech*, 2018, pp. 2718–2722.
- [19] Z.-Q. Wang and D. L. Wang, "Combining Spectral and Spatial Features for Deep Learning Based Blind Speaker Separation," *IEEE/ACM Trans. Audio, Speech, Lang. Process.*, vol. 27, no. 2, pp. 457–468, 2019.
- [20] S. Chakrabarty, D. L. Wang, and E. A. P. Habets, "Time-Frequency Masking Based Online Speech Enhancement with Multi-Channel Data using Convolutional Neural Networks," in *Proceedings of IWAENC*, 2018, pp. 476–480.
- [21] S. Chakrabarty and E. A. P. Habets, "Time-Frequency Masking Based Online Multi-Channel Speech Enhancement with Convolutional Recurrent Neural Networks," *IEEE J. Sel. Top. Signal Process.*, 2019.
- [22] N. Ma, T. May, and G. Brown, "Exploiting Deep Neural Networks and Head Movements for Robust Binaural Localization of Multiple Sources in Reverberant Environments," *IEEE/ACM Trans. Audio, Speech, Lang. Process.*, vol. 25, no. 12, pp. 2444–2453, 2017.
- [23] X. Xiao, S. Zhao, X. Zhong, D. L. Jones, E. S. Chng, and H. Li, "A Learning-Based Approach to Direction of Arrival Estimation in Noisy and Reverberant Environments," in *IEEE International Conference on Acoustics, Speech and Signal Processing*, 2015, pp. 2814–2818.
- [24] S. Chakrabarty and E. A.P. Habets, "Multi-Speaker DOA Estimation using Deep Convolutional Networks Trained with Noise Signals," *IEEE J. Sel. Top. Signal Process.*, vol. 13, no. 1, pp. 8–21, 2019.
- [25] E. L. Ferguson, S. B. Williams, and C. T. Jin, "Sound Source Localization in a Multipath Environment using Convolutional Neural Networks," in *IEEE International Conference on Acoustics, Speech and Signal Processing*, 2018, pp. 2386–2390.
- [26] D. Stoller, S. Ewert, and S. Dixon, "Wave-U-Net: A Multi-Scale Neural Network for End-to-End Audio Source Separation," in *Proceedings of ISMIR*, 2018, pp. 334–340.
- [27] N. Tawara, T. Kobayashi, and T. Ogawa, "Multi-Channel Speech Enhancement using Time-Domain Convolutional Denoising Auto-encoder," in *Proceedings of Interspeech*, 2019, pp. 86–90.
- [28] C.-L. Liu, S.-W. Fu, Y.-J. Lee, Y. Tsao, J.-W. Huang, and H.-M. Wang, "Multichannel Speech Enhancement by Raw Waveform-Mapping using Fully Convolutional Networks," in *arXiv preprint arXiv:1909.11909*, 2019.
- [29] Y. Luo and N. Mesgarani, "Real-time Single-channel Dereverberation and Separation with Time-Domain Audio Separation Network," in *Proceedings of Interspeech*, 2018, pp. 342–346.
- [30] D. Williamson, Y. Wang, and D. L. Wang, "Complex Ratio Masking for Monaural Speech Separation," *IEEE/ACM Trans. Audio, Speech, Lang. Process.*, pp. 483–492, 2016.
- [31] S.-W. Fu *et al.*, "Complex Spectrogram Enhancement By Convolutional Neural Network with Multi-Metrics Learning," in *IEEE International Workshop on Machine Learning for Signal Processing*, 2017, pp. 1–6.
- [32] K. Tan and D. L. Wang, "Complex Spectral Mapping with A Convolutional Recurrent Network for Monaural Speech Enhancement," in *IEEE International Conference on Acoustics, Speech and Signal Processing*, 2019, vol. 2019-May, pp. 6865–6869.
- [33] S. Wisdom *et al.*, "Differentiable Consistency Constraints for Improved Deep Speech Enhancement," in *IEEE International Conference on Acoustics, Speech and Signal Processing*, 2019, vol. 2019, pp. 900–904.
- [34] Z.-Q. Wang, J. Le Roux, D. L. Wang, and J. R. Hershey, "End-to-End Speech Separation with Unfolded Iterative Phase Reconstruction," in *Proceedings of Interspeech*, 2018, pp. 2708–2712.
- [35] Z.-Q. Wang, K. Tan, and D. L. Wang, "Deep Learning Based Phase Reconstruction for Speaker Separation: A Trigonometric Perspective," in *IEEE International Conference on Acoustics, Speech and Signal Processing*, 2019, pp. 71–75.
- [36] K. Kinoshita *et al.*, "A Summary of the REVERB Challenge: State-of-the-Art and Remaining Challenges in Reverberant Speech Processing Research," *EURASIP J. Adv. Signal Process.*, no. 1, pp. 1–19, 2016.
- [37] J. Le Roux, S. Wisdom, H. Erdogan, and J. R. Hershey, "SDR – Half-Baked or Well Done?," in *IEEE International Conference on Acoustics, Speech and Signal Processing*, 2019, pp. 626–630.
- [38] O. Ronneberger, P. Fischer, and T. Brox, "U-Net: Convolutional Networks for Biomedical Image Segmentation," in *Proceedings of MICCAI*, 2015.
- [39] G. Huang, Z. Liu, L. V. D. Maaten, and K. Q. Weinberger, "Densely Connected Convolutional Networks," in *IEEE Conference on Computer Vision and Pattern Recognition*, 2017.
- [40] Z.-Q. Wang and D. L. Wang, "Deep Learning Based Target Cancellation for Speech Dereverberation," *IEEE/ACM Trans. Audio, Speech Lang. Process.*, 2020.
- [41] H. Erdogan, J. R. Hershey, S. Watanabe, and J. Le Roux, "Phase-Sensitive and Recognition-Boosted Speech Separation using Deep Recurrent Neural Networks," in *IEEE International Conference on Acoustics, Speech and Signal Processing*, 2015, pp. 708–712.